processes

MDPI

Article

Study of H_2S Removal Capability from Simulated Biogas by Using Waste-Derived Adsorbent Materials

Hua Lun Zhu [1], Davide Papurello [2,3], Marta Gandiglio [2,3], Andrea Lanzini [2,3], Isil Akpinar [4,5], Paul R. Shearing [4], George Manos [4], Dan J.L. Brett [4] and Ye Shui Zhang [4,*]

1 Department of Chemical Engineering, Imperial College London, London SW7 2AZ, UK; h.zhu16@imperial.ac.uk
2 Energy Department (DENERG), Politecnico di Torino, Corso Duca degli Abruzzi, 24, 10129 Turin, Italy; d016886@polito.it (D.P.); marta.gandiglio@polito.it (M.G.); andrea.lanzini@polito.it (A.L.)
3 Energy Center, Politecnico di Torino, Via Borsellino, 38, 10129 Turin, Italy
4 Department of Chemical Engineering, University College London, Torrington Place, London WC1E 7JE, UK; isil.akpinar.13@ucl.ac.uk (I.A.); p.shearing@ucl.ac.uk (P.R.S.); g.manos@ucl.ac.uk (G.M.); d.brett@ucl.ac.uk (D.J.L.B.)
5 Department of Environmental Engineering, Aksarary University, Aksaray 68100, Turkey
* Correspondence: yeshui.zhang@ucl.ac.uk

Received: 19 July 2020; Accepted: 20 August 2020; Published: 24 August 2020

Abstract: Three waste-derived adsorbent materials (wood-derived biochar, sludge-derived activated carbon and activated ash) were pre-activated at the laboratory scale to apply them for the removal of H_2S from a biogas stream. The H_2S removal capabilities of each material were measured by a mass spectrometer, to detect the H_2S concentration after the adsorption in an ambient environment. The activated ash adsorbent has the highest removal capacity at 3.22 mg_{H2S} g^{-1}, while wood-derived biochar has slightly lower H_2S removal capability (2.2 mg_{H2S} g^{-1}). The physicochemical properties of pristine and spent materials were characterized by the thermogravimetric analyzer, elemental analysis, X-ray fluorescence spectroscopy and N_2 adsorption and desorption. Wood-derived biochar is a highly porous material that adsorbs H_2S by physical adsorption of the mesoporous structure. Activated ash is a non-porous material which adsorbs H_2S by the reaction between the alkaline compositions and H_2S. This study shows the great potential to apply waste-derived adsorbent materials to purify a biogas stream by removing H_2S.

Keywords: activated carbon; waste; adsorption; biochar; H_2S; circular economy; catalysis

1. Introduction

Facing significant environmental degradation, with continuous increases in natural resource consumption, the new attention on green growth, but especially on low carbon development, turns out to be crucial to the circular economy (CE) approach. In this field, pyrolysis and gasification of carbonaceous materials such as waste tires, waste plastics and crude glycerol from the biodiesel industry have potential to become profitable liquid, gaseous and solid products [1,2]. Liquid products containing naphtha, tars and phenols can be applied straight away or upgraded as fuels [3]. Gas products containing syngas (H_2 and CO), methane and others can also be used as fuels depending on their purity [4,5] in several energy generators, such as: internal combustion engines (ICE) [6], microturbines (MT) [7] and highly efficient solid oxide fuel cell (SOFC) systems [8]. Solid products, on the other hand, are mainly chars that can be upgraded to activated carbons through chemical and/or physical processes [9]. Biogas or in general gas products play the vital role of fulfilling the energy demand worldwide, which could be applied in heat and power generation and vehicle fuel with proper

purification [10]. To upgrade gas production for further application, catalysts are normally used, for example, to enhance hydrogen production [11–14] and to play an important role in gasification processes [15]. Transition metals are considered good catalysts for the reforming of hydrocarbons [16]. Nickel-based catalysts are most frequently used in the production of hydrogen by the thermochemical processing of plastics and biomass primarily because of their stability at high temperatures and high selectivity for hydrogen [17–19]. Hydrogen sulfide (H_2S) as one of the impurities was found in the biogas stream since the sulfur content in the feedstock was within a range of 100–200 ppm(v) [20]. H_2S could lead to catalyst deactivation due to the corrosion of metal surfaces, the poisoning of catalysts and sulfur dioxide formation in the combustion processes [5,21]. Elbaba et al. [22] found that the deactivation of a Ni/Al_2O_3 catalyst in the gasification of a waste tire for hydrogen production was due to sulfur poisoning and carbon deposition. As H_2S would hinder the application of biogas economically and environmentally [10], it is strictly necessary to remove the H_2S from the biogas stream to improve the purity and avoid catalyst deactivation.

Many of the adsorbents have been investigated for gas desulphurization, such as zeolite [23], activated carbons [24–28], metal oxides supported by mesoporous silica [29], graphite oxide [30], hydroxyapatite [31] and functionalized activated carbon [32]. Furthermore, specific modifications of the adsorbents are normally required to improve the adsorption efficiency which are not environmentally friendly and also increase the cost of the adsorbents [33], such as caustic or metal impregnation [32,34,35]. Alternatively, other waste-derived materials such as pyrolysis biochar, sludge collected from the wastewater treatment plant and ash collected from the biomass gasifier will be investigated as adsorbents to remove H_2S from the biogas stream.

Few of the studies have been done by using waste-derived materials to purify biogas [33,36,37]. Hervy et al. [33] investigated the H_2S removal efficiency of pyrolysis biochar and sludge at ambient temperature in various dry gas matrices that include N_2, air and syngas. The results demonstrated the activated chars derived from waste-derived materials could effectively play the role of syngas desulfurization under dry atmosphere, which is eco-friendly and affordable. Florent et al. [36] synthesized sewage sludge/porous carbon composites as H_2S adsorbents. The good H_2S removal performance of sludge-derived adsorbents in gas desulfurization relates to the surface basicity due to the high content of calcium and magnesium, and also the oxidation reactions with an inorganic phase such as iron or copper species [38]. Juared et al. [37] investigated the H_2S removal ability of biomass ash and concluded it could be used for the removal of H_2S from biogas in small and medium biogas plants. Ahmad et al. [10] reviewed the different waste-derived materials as adsorbents (sewage sludge, food waste, forestry waste, fly ash and industrial waste). They stated there is a big potential to utilize these materials as alternative commercial H_2S adsorbents with extensive studies.

Considering the complexity and large range of waste materials as potential H_2S removal adsorbents, there is a need to understand the mechanism of each type of adsorbent material for H_2S removal to find an eco-friendly and effective adsorbent. This work aims to compare the H_2S removal ability of three different waste-derived adsorbents, wood-derived biochar (WDC), sludge-derived carbon (SDC) and activated ash (AA). The objectives were included the H_2S adsorption capability and the H_2S adsorption mechanism by using these three waste-derived adsorbents in the field of the new circular economy approach.

2. Materials and Methods

2.1. Materials

The wood-derived biochar (WDC) was collected from a 200 kWe wood pyrolysis reactor (Gruppo RM Impianti Srl, Giarre, Italy) with the pyrolysis temperature at ~450 °C. The ash sample used in this work is from a forestry wood chips boiler (3.3 MW, Viessman, Allendorf Germany). The activation of WDC and wood ash was carried out in a 500 We tubular furnace (C.I.T.T., Milano Italy). The raw

samples were heated to 700 °C with a ramp rate at 7 °C min^{-1}. Carbon dioxide was the activating agent with a constant flow rate of 100 mL min^{-1} for 60 min under isothermal conditions.

The sludge-derived activated carbon (SDC) was prepared from an anaerobically digested and dried sewage sludge collected from the SMAT wastewater treatment plant (WWTP) site (Castiglione Torinese, Italy). Physical activation of milled sludge (~1 mm) was carried out in a stainless-steel reactor with diameter ~34 mm and ~570 mm in length, which was externally heated by a tubular furnace to 600 °C. These low-temperature values were selected to simulate a direct coupling with SOFC engine gas exhausts [39]. Nitrogen was the purge gas during the pyrolysis of the raw sludge sample for physical activation, and carbon dioxide and air were the activating agents. The activated samples were ground to obtain grain size ~400 µm using a vibratory sieve shaker (Fritsch, Germany).

2.2. Experimental Set-Up

The schematic diagram for testing the H_2S removal capability of the three selected samples is shown in Figure 1. A mixture of gases (CH_4-to-CO_2 ratio at 1.5 and H_2S at 200 ppm(v)) was used as simulated biogas. The mixture of the gas inlet was controlled by three individual specific mass flow controllers (Bronkhorst EL-FLOW, NL), to simulate an average biogas mixture deriving from the anaerobic digestion of organic waste. This concentration is representative of real biogas as reported in the literature [40–42]. These sorbent materials were placed in Teflon tubes with an internal diameter of 25 mm. The aspect ratio between the sorbent height and plastic tube inner diameter is ~8.33. To remove residual gases inside the pores, the samples were pre-treated using 200 NmL min^{-1} N_2 flow for 30 min at 120 °C. A gas flow of 919.9 NmL min^{-1} was used for the H_2S removal performance testing. The gas outlet was analyzed by a mass spectrometer (MS) (QGA, Hiden Analytical Ltd., UK) to monitor the online H_2S concentration. The H_2S removal tests were repeated for each sample to prove the reliability of the H_2S removal capability.

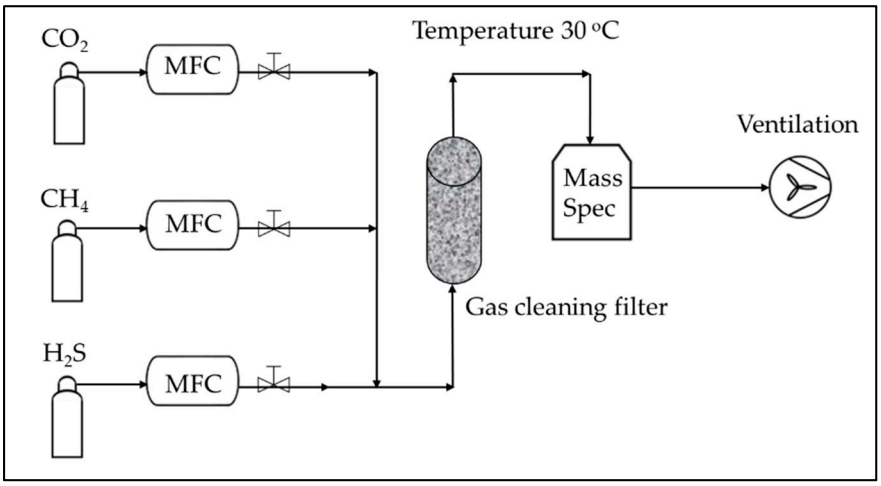

Figure 1. Schematic diagram of the H_2S removal from a simulated biogas stream with wood-derived activated carbon, sludge-derived activated carbon and activated ash.

2.3. Methodology

The H_2S adsorption capacity in terms of mg g^{-1} for H_2S removal was calculated based on Equation (1) [43,44], which was corrected considering that the area enclosed by the breakthrough curve and the saturation line up to t_1 is estimated by the difference between the rectangle (t_1 (h) C_{in} (ppmv)) and the triangle (0.5 ($t_1 - t_0$) (h) 1 (ppmv)) areas:

$$C_{ads} = \frac{Q_{tot} \times MW \times [C_{in} \times t_1 - (t_1 - t_0) \times 0.5]}{V_m \times m \times 10^3} \quad (1)$$

where:

- t_0, breakthrough time at the last detection of 0–0.5 ppmv (h);
- t_1, breakthrough time when the outlet H_2S concentration is 1 ppmv (h);
- Q_{tot} = total gas flow rate (NL h^{-1});
- MW = molecular weight of the trace compound removed (g mol^{-1});
- C_{in} = inlet trace compound concentration (ppm(v));
- V_m = molar volume (22.414 NL mol^{-1});
- m = mass of sorbent (g).

2.4. Characterization Methods

Elemental analysis: The elemental analysis for virgin and spent samples was obtained from SOCOTEC, UK. The oxygen content was calculated by the difference. The chemical composition of each pristine and spent adsorbent material was analyzed by a Panalytical X-ray fluorescence spectroscopy (XRF) Epsilon 3XL.

Scanning Electron Microscopy: A Zeiss EVO 10 scanning electron microscope (SEM) was used to characterize both the virgin adsorbents.

Thermogravimetric analysis: The ash contents of the virgin samples were estimated by using a Netzsch STA 2500 Regulus thermogravimetric analyzer (TGA). The heating program started with 10 °C min^{-1} to 120 °C and holding for 30 min to remove the moisture content in the virgin samples in the presence of nitrogen. Then, the sample was heated to 800 °C with 10 °C min^{-1} ramp rate to combust the organic compound. The air flow was constantly at 40 mL min^{-1}. The same TGA coupled with a Hiden Analytical QGA Mass spectrometer was used to study the sulfur compounds' decomposition behaviors with nitrogen as a constantly purged gas.

pH measurement: The pH values of the three virgin samples and the spent samples were measured to compare the pH evaluation of the three different samples after the H_2S adsorption. Approximately 0.4 g of each of dry sample was added in 20 mL distilled water to make the homogenous suspension for pH measurement, by using a Hanna Instruments pH meter.

Physical adsorption and desorption: The porous properties of the virgin char and spent samples were determined by measuring the nitrogen adsorption and desorption isotherms from the samples at equilibrium vapor pressure using the static volumetric method. Nitrogen adsorption–desorption isotherms were recorded at 77 K using a Micromeritics 3Flex surface characterization analyzer. The samples were degassed at 300 °C overnight. Specific surface areas were determined according to the Brunauer, Emmett and Teller (BET) model [45,46], with pore diameters, volumes and distributions determined through Barrett–Joyner–Halenda (BJH) analysis [47].

3. Results and Discussion

3.1. H_2S Removal Capacity

The H_2S removal efficiency tests of three adsorbents were carried out in the simulated biogas stream. The H_2S removal capacity of each adsorbent is listed in Table 1, which shows the AA with the highest removal capacity at 3.22 mg_{H2S} g^{-1} and SDC with the lowest removal capacity at 0.1 mg_{H2S} g^{-1}. Each of the adsorbent materials has been repeated twice for the H_2S removal test to confirm the experimental reproducibility.

Table 1. H_2S adsorption capacities of wood-derived biochar (WDC), sludge-derived activated carbon (SDC) and activated ash (AA).

Sample	WDC	SDC	AA
C_{ads} (mg_{H2S} g^{-1})	2.2 +/− 0.05	0.1 +/− 0.01	3.22 +/− 0.06

3.2. Characterizations of Adsorbents

Figure 2 is the SEM micrographs of virgin adsorbents which show the morphology of the adsorbent particles. Figure 2a,b are the SEM micrographs of virgin WDC adsorbents, the particles have cracking features. Figure 2c,d are the SEM micrographs of virgin SDC that present as smaller particles supported on the larger particles. Figure 2e,f are the SEM micrographs of virgin AA which demonstrate the large cluster of fine power. Figure 3 is the thermogravimetric analysis of the three raw adsorbents WDC, SDC and AA. The residue left after temperature-programmed oxidation is ash, whereas the weight loss is caused by the oxidation of organic composition. The results show the ash contents ranking of the three adsorbents is AA > SDC > WDC and the ranking of organic components is in a reverse direction. The results are consistent with the elemental analysis results listed in Table 2, where the carbon compositions for three raw adsorbents is ranked as WDC > SDC > AA. This result could explain why the H_2S removal capacity of WDC is higher than SDC in Table 1, because the porous carbon content in WDC is 88.93% which is much higher than the content in SDC, which is 33.94%. The porosity of carbon could also be supported by the nitrogen adsorption and desorption analysis shown in Table 4, where the WDC has the highest surface area and total pore volume that are 210.18 m^2 g^{-1} and 0.5 cm^3 g^{-1}, respectively.

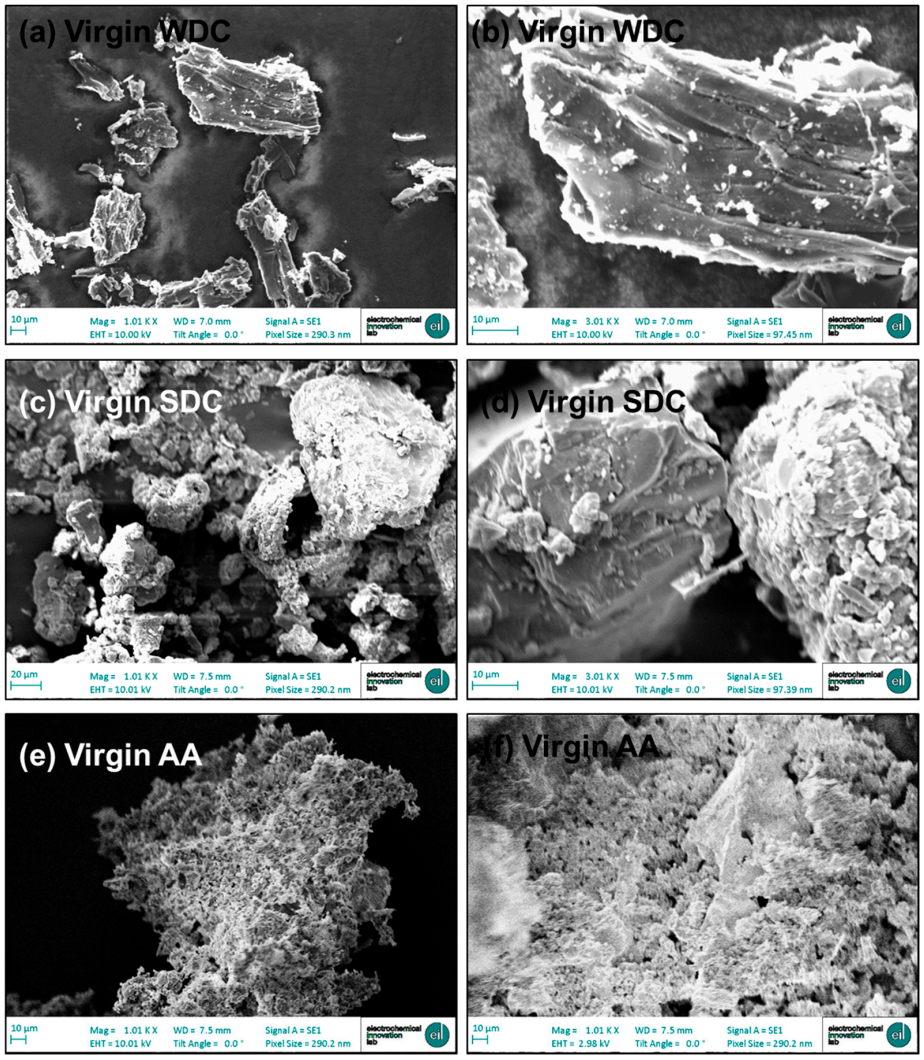

Figure 2. SEM micrographs of virgin WDC (**a**,**b**); virgin SDC (**c**,**d**); virgin AA (**e**,**f**).

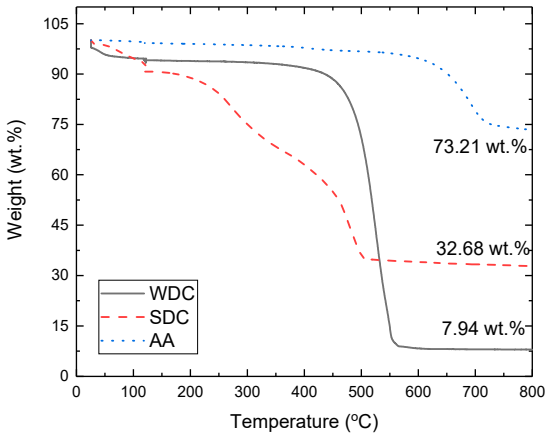

Figure 3. Ash contents for virgin WDC, SDC and AA.

Although SDC contains a higher amount of carbon (33.94 wt.%) compared with AA (7.42 wt.%) in Table 2, the H_2S removal capacity of SDC (0.1 mg_{H2S} g^{-1}) is lower than AA (3.22 mg_{H2S} g^{-1}) and this is related to the high ash content in AA (73.21 wt.%), as shown in Table 2. It has been reported that the incineration residues that contain many compounds would form sulfides as H_2S-trap materials which can react with H_2S at ambient temperature, such as manganese, zinc, copper and iron [37]. The porosity analysis results shown in Table 4 can also prove there is no significant difference between SDC and AA in terms of surface area and total pore volume.

Table 2. Elemental composition, pH and ash content of virgin and spent adsorbent samples.

Sample Name	Elemental Analysis (wt.%)					pH	Ash (wt.%)
	C	H	N	O	S		
WDC	88.93	<0.08	0.11	10.88	-	7.2	7.94
Spent WDC	95.58	<0.08	0.16	4.18	-	7.3	
SDC	33.94	4.2	5.18	56.68	-	7.9	32.68
Spent SDC	34.76	4.28	5.13	55.83	-	7.6	
Activated ash (AA)	7.42	<0.08	<0.08	92.42	-	8.8	73.21
Spent AA	7.37	<0.08	<0.08	92.47	-	8.4	

Table 2 lists the elemental composition and pH values for the virgin and spent adsorbent materials. The CHNO compositions for virgin and spent WDC adsorbents are similar, and the pH value was slightly increased from 7.2 to 7.3 which indicates the chemical reaction has mostly not happened during the adsorption of H_2S by WDC. The pH values for spent SDC and AA are slightly lower than the virgin adsorbents that indicate the chemical reaction occurred between the H_2S and the alkaline compositions. In other words, the chemical adsorption of H_2S by SDC and AA is more dominated than WDC.

Table 3 presents the ash composition of the pristine and spent adsorbent materials by XRF which prove the existence of alkaline compositions, such as Fe, Cu, Mn and Ca. Calcium is the main mineral species in WDC and AA adsorbents, and iron is the main mineral species in SDC adsorbents. Juarez et al. [37] reported that alkaline or pH-neutral waste contain sulfites or a mixture of Fe-II, Fe-III, Mn-II, Cu-I, Cu-II and Zn-II which play the role of potential H_2S-trap materials. The possible reaction for the H_2S removal by SDC and AA adsorbents could relate to the "primary" and "secondary" reactions [37]. The primary dissociation reactions include Reactions (2) and (3), and the suggested secondary sulfidation reactions could be (3)–(11) [37,48,49].

$$OH^- + H_2S = HS^- + H_2O \quad (2)$$

$$HS^- + OH^- = S^{2-} + H_2O \quad (3)$$

$$FeO + H_2S = FeS + H_2O \quad (4)$$

$$Fe_2O_3 + 3H_2S = Fe_2S_3 + 3H_2O \quad (5)$$

$$2Fe(OH)_3 + 3H_2S = Fe_2S_3 + 6H_2O \quad (6)$$

$$2FeOOH + 3H_2S = Fe_2S_3 + 4H_2O \quad (7)$$

$$2HS^- + 4HSO_3^- = 3S_2O_3^{-2} + 3H_2O \quad (8)$$

$$2HS^- + HSO_3^- = \frac{3}{8}S_8 + 3OH^- \quad (9)$$

$$S^{2-} + nS = S_{n+1}^{2-} \quad (10)$$

$$MnO + H_2S = MnS + H_2O\ (Same\ with\ Cy,\ Ca\ and\ Ni) \quad (11)$$

Ducom et al. [50] reported the primary reactions (Equations (2) and (3)) are acid–base reactions since H_2S is hydrophilic and dissociates in aqueous solution. The primary reactions occur very fast which are not the dominant reaction for H_2S removal. Sarperi et al. explained the possible Fe sulfidation Reactions (4) and (5) [37]. The ash adsorbents may also contain hydrous ferrous oxide (HFO) and goethite (FeOOH) with a high specific surface area which will react with H_2S as shown in Equations (6) and (7) [51]. Juarez et al. [37] suggested that Reactions (8)–(10) between H_2S and sulfites will form polysulfides and elemental S_8 based on others' research [52,53].

Table 3. Compositions of pristine and spent adsorbents materials detected by XRF.

Compositions (wt.%)	WDC	Spent WDC	SDC	Spent SDC	AA	Spent AA
Mg	0.31	0.36	0.50	0.47	0.44	0.42
Al	nd	nd	2.72	2.68	1.78	1.70
Si	0.36	0.36	6.83	6.84	2.66	2.54
P	0.89	0.86	7.77	7.57	0.63	0.65
S	0.95	9.05	9.38	8.64	0.73	0.79
Cl	0.24	0.92	0.31	0.30	0.27	0.27
K	25.99	22.85	2.25	2.24	11.74	12.19
Ti	0.56	0.42	1.41	1.40	0.69	0.42
Ca	61.57	59.15	19.77	19.63	78.12	78.20
Fe	3.27	0.72	45.15	46.27	1.91	1.86
Mn	5.09	4.75	0.22	0.20	0.43	0.36
Zn	nd	0.19	1.62	1.65	0.13	0.13
Cu	nd	nd	0.63	0.63	nd	nd
Ni	nd	nd	0.29	0.30	nd	nd
Sr	nd	nd	0.31	0.31	0.23	0.23
Cr	nd	nd	0.20	0.21	nd	nd
Eu	nd	nd	0.12	0.13	nd	nd
Total (wt.%)	99.22	99.44	98.96	98.98	98.98	99.05

nd: not detected by XRF or concentration less than 0.1 wt.%.

Table 4 shows the porosity of the virgin and spent waste-derived adsorbent materials. The surface area of WDC decreased significantly from 210.18 to 96.95 $m^2\ g^{-1}$ after the H_2S removal. This could explain the certain amount of H_2S that was adsorbed by the porosity of WDC. However, there is no significant change of surface area and total pore volume for SDC and AA would also support the conclusion drawn earlier that the H_2S removal capacity of WDC and AA was dominated by the chemical reactions rather than the physical adsorption. Although the AA adsorbent is not as porous as WDC, the surface area and total pore volume also decreased slightly which indicates that physical adsorption also happened. In Table 4, the average pore diameter for virgin WDC is 19.64 Å, which indicates the presence of mesopores. Figure 4 illustrates the N_2 adsorption and desorption isotherms of (a) virgin WDC, (b) spent WDC, (c) virgin SDC, (d) spent WDC, (c) virgin AA and (f) spent AA adsorbent materials. According to the BJH pore size distribution illustrated in Figure 5a, the presence

of mesopore distributions in the WDC sample can be confirmed. The mesopore has been reported as the active site for H_2S adsorption [33].

Table 4. Surface area, total pore volume and average pore diameter of virgin and spent adsorbents.

Sample	Surface Area (m^2 g^{-1})	* Total Pore Volume (cm^3 g^{-1})	Average Pore Diameter (Å)
WDC	210.18	0.50	19.64
Spent WDC	96.95	0.14	19.65
SDC	1.89	0.004	16.58
Spent SDC	1.59	0.004	16.60
Activated ash (AA)	9.38	0.011	96.29
Spent AA	4.66	0.0086	110.27

* Single point desorption total pore volume of pores less than 403.122 Å diameter at P/Po = 0.95.

Figure 4a,b,e,f exhibit kinds of type IV or V isotherms according to the IUPAC classification, indicative of the presence of mesopores within the virgin and spent WDC and AA samples [54,55]. The hysteresis for virgin and spent WDC and AA samples adsorption isotherms shown in Figure 4a,b,e,f could relate to the morphological properties of the sample. The morphological properties have been summarized by other researchers which include the pore size distribution, pore geometry and connectivity of the porous materials [55,56]. The shape of the adsorption hysteresis loop exhibited similar as H_3 shape indicates the porous material could have slit-shaped pores with two ends open, which can be supported by other researchers' findings [55,57,58]. The slope associated with the hysteresis loop of the adsorption/desorption curves is related to the tensile strength effect [54,55,59]. The highlighted hysteresis curves that are shown in Figure 4b,f indicate the low-pressure hysteresis due to the volume change of the adsorbent. It could be caused by the swelling of the non-rigid pores in the spent SDC and AA adsorbent materials, or the pores have been occupied irreversibly by the similarly sized molecules [55,60].

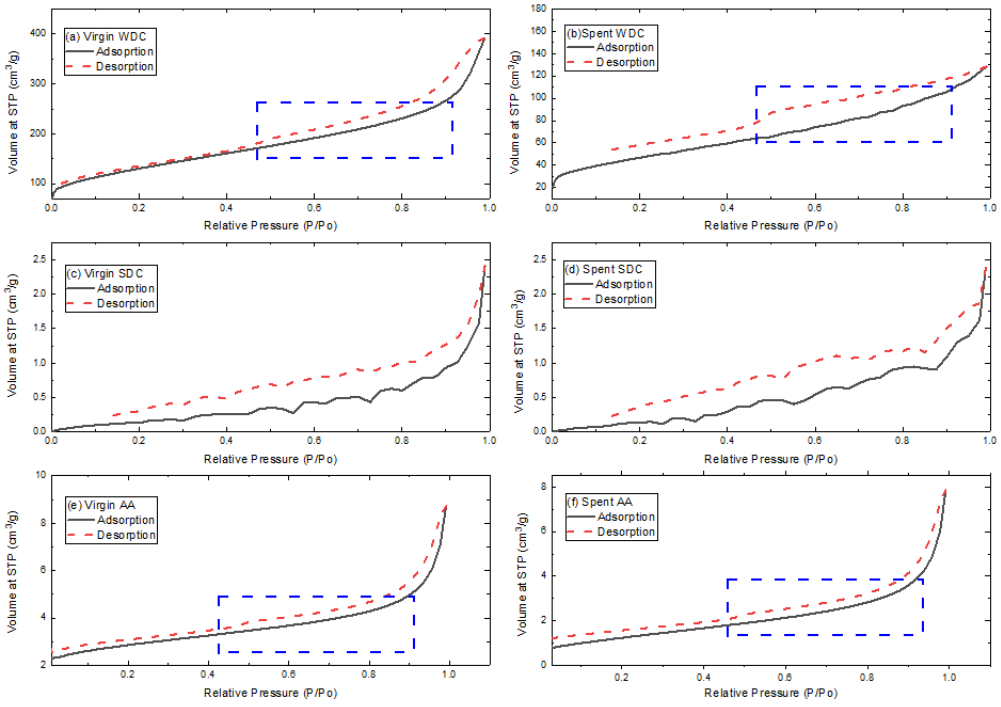

Figure 4. N_2 adsorption and desorption isotherms of (**a**) virgin WDC, (**b**) spent WDC, (**c**) virgin SDC, (**d**) spent WDC, (**e**) virgin AA and (**f**) spent AA adsorbent materials.

Figure 5a,b illustrate the pore size distributions of the virgin and spent WDC adsorbents. According to the peak, peak A diminished significantly for the spent WDC in Figure 5b compared with the virgin WDC shown in Figure 5a, and the total pore volume decreased from 0.50 to 0.14 cm^3 g^{-1} as shown in Table 4, indicating that the mesopore size ~38 Å contributes to H_2S adsorption. The peak A in Figure 5c,d has no obvious change after H_2S adsorption which could support the assumption made earlier that the chemical reaction is more dominated by the H_2S removal from the simulated biogas stream by using the AA adsorbent material.

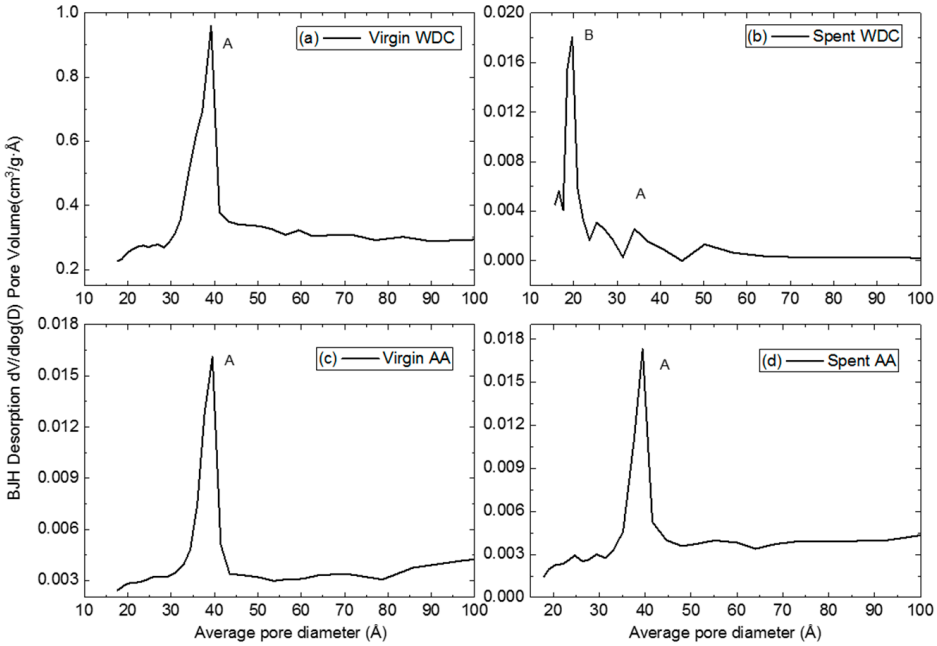

Figure 5. Barrett–Joyner–Halenda (BJH) pore size distribution of (**a**) virgin WDC, (**b**) spent WDC, (**c**) virgin AA and (**d**) spent AA adsorbent materials.

In Figure 6a–d, peak A in the derivative thermal gravimetric (DTG) curves at temperature ~100 °C indicates the removal of moisture in the samples. The results reveal that WDC and SDC contain such an amount of moisture, but not the AA sample, according to the DTG and mass spectrometry results in Figure 6. In Figure 6a–d, peak B at ~620 °C and peak C at temperature ~780 °C, and in Figure 6e,f, peak A at temperature ~750 °C and peak B at temperature ~780 °C are associated with the emission of CO_2 from the adsorbent materials. The results are also supported by Hervy et al.'s research [33], that the CO_2 emitted from adsorbents under the same TGA program at temperatures ~200, 620 and 750 °C; the H_2S emitted from adsorbents at temperature ~370 °C; and the SO_2 emitted at temperatures ~285 and 370 °C. There is no obvious SO_2 or H_2S emitted from the virgin and spent adsorbent materials could cause by the relatively small amount that the equipment is not sensitive enough.

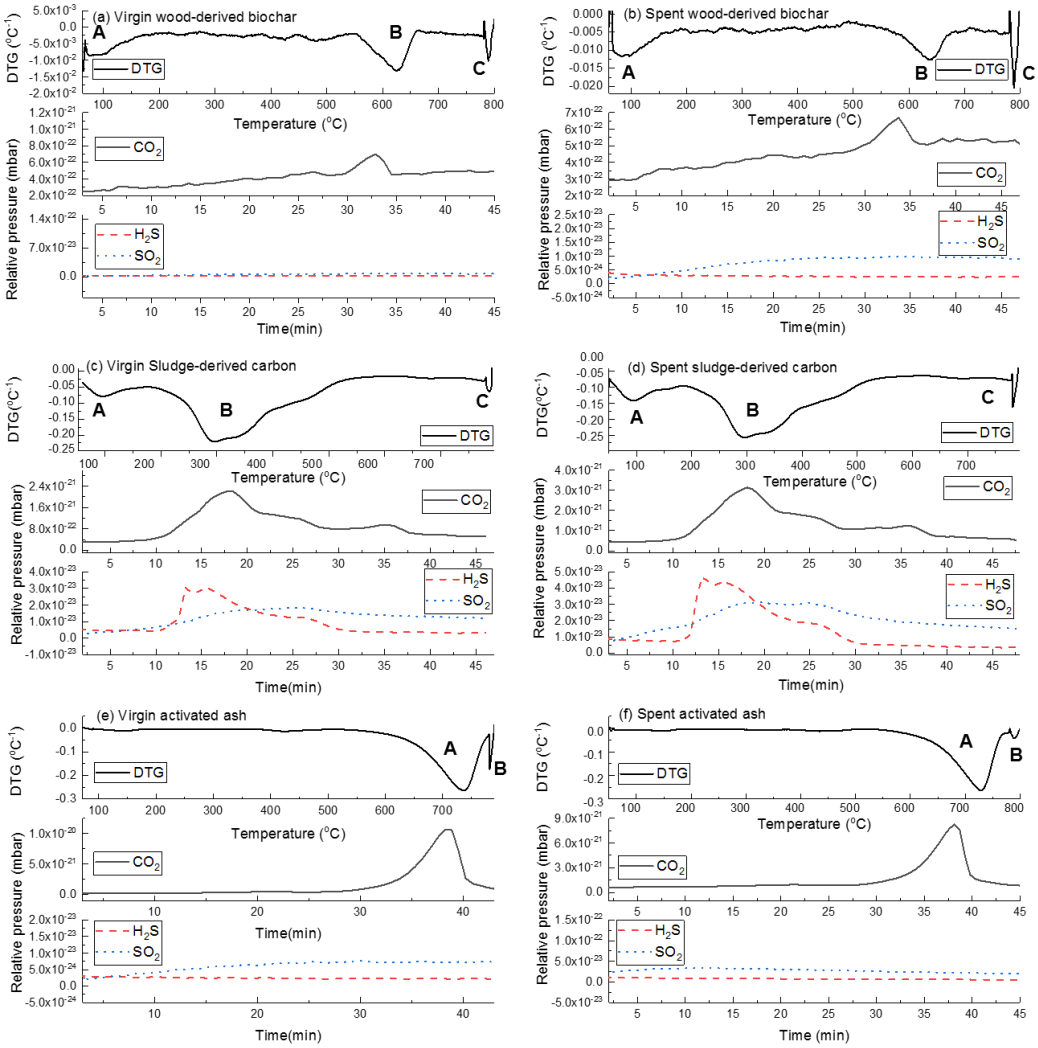

Figure 6. DTG-MS analysis of (**a**) virgin WDC, (**b**) spent WDC, (**c**) virgin SDC, (**d**) spent SDC, (**e**) virgin AA and (**f**) spent AA under N_2.

4. Conclusions

This work compared the H_2S removal capability of three types of adsorbent material from waste (wood-derived biochar, sludge-derived activated carbon and activated ash) in ambient temperature. The raw adsorbent materials were pre-activated under certain activation methods. A simulated biogas stream with the CH_4-to-CO_2 ratio at 1.5 and H_2S concentration at 200 ppm(v) was used to test the H_2S removal efficiency of each adsorbent material. The concentration of H_2S after the adsorption was measured by an MS. The MS result shows that the AA adsorbent has the highest removal capacity at 3.22 mg_{H2S} g^{-1} and WDC has slightly lower H_2S removal capability at 2.2 mg_{H2S} g^{-1}. The TGA result shows that the ash residues composition of each adsorbent materials is ranked as AA (73.21 wt.%) > SDC (37.68 wt.%) > WDC (7.94 wt.%). The ash content results are also supported by the elemental analysis in which the carbon content of each adsorbent material is ranked as WDC (88.93 wt.%) > SDC (33.97 wt.%) > AA (7.42 wt.%). The ash composition was measured by XRF which shows the existence of alkaline mineral species in all adsorbent materials, such as Fe, Cu and Mn. The main mineral species in the WDC and AA adsorbents is Ca, and the main mineral species in the SDC adsorbent is Fe. WDC has relatively higher H_2S removal capability (2.2 mg_{H2S} g^{-1}) compared with SDC (0.1 mg_{H2S} g^{-1}), which is due to the physical adsorption by its high porosity, so that the surface area of WDC is 210.18 m^2 g^{-1}. The mesopores play the most important role in adsorbing H_2S. AA has the highest capability to remove H_2S, which is due to the high content of ash residues which contain an alkaline

mineral species that is more dominant in the H_2S removal rather than physical adsorption. In summary, this study indicates the potential to apply waste-derived adsorbent materials to remove H_2S from a biogas stream, especially by using WDC and AA.

Author Contributions: Conceptualization, Y.S.Z. and D.P.; methodology, H.L.Z. and Y.S.Z.; software, D.P. and Y.S.Z.; validation, D.P., Y.S.Z. and H.L.Z.; formal analysis, H.L.Z. and Y.S.Z.; investigation, M.G. and A.L.; resources, D.P., M.G. and A.L.; data curation, D.P., Y.S.Z. and H.L.Z.; writing—original draft preparation, Y.S.Z. and H.L.Z.; writing—D.P., M.G., A.L., I.A., P.R.S., D.J.L.B. and G.M.; visualization, H.L.Z. and Y.S.Z.; supervision, Y.S.Z.; project administration, H.L.Z.; funding acquisition, Y.S.Z., G.M. and D.J.L.B. All authors have read and agreed to the published version of the manuscript.

Funding: This work was part of the research activities carried out in the framework of the "European Biofuels Research Infrastructure for Sharing Knowledge 2 (BRISK2)" project under grant agreement 731101 (https://brisk2.eu/) and the European Commission is acknowledged for co-funding the work.

Conflicts of Interest: The authors declare no conflict of interest.

References

1. Ahmed, I.; Gupta, A. Syngas yield during pyrolysis and steam gasification of paper. *Appl. Energy* **2009**, *86*, 1813–1821. [CrossRef]
2. Williams, P.T. *Waste Treatment and Disposal*; John Wiley & Sons: Chichester, UK, 2005.
3. Demirbas, A. Effects of temperature and particle size on bio-char yield from pyrolysis of agricultural residues. *J. Anal. Appl. Pyrolysis* **2004**, *72*, 243–248. [CrossRef]
4. Kodera, Y.; Ishihara, Y.; Kuroki, T. Novel process for recycling waste plastics to fuel gas using a moving-bed reactor. *Energy Fuels* **2006**, *20*, 155–158. [CrossRef]
5. Woolcock, P.J.; Brown, R.C. A review of cleaning technologies for biomass-derived syngas. *Biomass Bioenergy* **2013**, *52*, 54–84. [CrossRef]
6. Dobslaw, D.; Engesser, K.-H.; Störk, H.; Gerl, T. Low-cost process for emission abatement of biogas internal combustion engines. *J. Clean. Prod* **2019**, *227*, 1079–1092. [CrossRef]
7. Baudoin, S.; Vechiu, I.; Camblong, H.; Vinassa, J.-M.; Barelli, L. Sizing and control of a solid oxide fuel cell/gas microturbine hybrid power system using a unique inverter for rural microgrid integration. *Appl. Energy* **2016**, *176*, 272–281. [CrossRef]
8. Abdelkareem, M.A.; Tanveer, W.H.; Sayed, E.T.; Assad, M.E.H.; Allagui, A.; Cha, S. On the technical challenges affecting the performance of direct internal reforming biogas solid oxide fuel cells. *Renew. Sustain. Energy Rev.* **2019**, *101*, 361–375. [CrossRef]
9. Coppola, G.; Papurello, D. Biogas cleaning: Activated carbon regeneration for h2s removal. *Clean Technol.* **2019**, *1*, 40–57. [CrossRef]
10. Ahmad, W.; Sethupathi, S.; Kanadasan, G.; Lau, L.C.; Kanthasamy, R. A review on the removal of hydrogen sulfide from biogas by adsorption using sorbents derived from waste. *Rev. Chem. Eng.* **2019**. [CrossRef]
11. He, M.; Xiao, B.; Hu, Z.; Liu, S.; Guo, X.; Luo, S. Syngas production from catalytic gasification of waste polyethylene: Influence of temperature on gas yield and composition. *Int. J. Hydrog. Energy* **2009**, *34*, 1342–1348. [CrossRef]
12. Coll, R.; Salvadó, J.; Farriol, X.; Montané, D. Steam reforming model compounds of biomass gasification tars: Conversion at different operating conditions and tendency towards coke formation. *Fuel Process. Technol.* **2001**, *74*, 19–31. [CrossRef]
13. Lee, D.C.; Mikulec, F.V.; Korgel, B.A. Carbon nanotube synthesis in supercritical toluene. *J. Am. Chem. Soc.* **2004**, *126*, 4951–4957. [CrossRef] [PubMed]
14. Lakhapatri, S.L.; Abraham, M.A. Deactivation due to sulfur poisoning and carbon deposition on rh-ni/al2o3 catalyst during steam reforming of sulfur-doped n-hexadecane. *Appl. Catal. A Gen.* **2009**, *364*, 113–121. [CrossRef]
15. Chiodo, V.; Urbani, F.; Galvagno, A.; Mondello, N.; Freni, S. Analysis of biogas reforming process for molten carbonate fuel cells. *J. Power Sources* **2012**, *206*, 215–221. [CrossRef]
16. Abu El-Rub, Z.; Bramer, E.A.; Brem, G. Review of catalysts for tar elimination in biomass gasification processes. *Ind. Eng. Chem. Res.* **2004**, *43*, 6911–6919. [CrossRef]

17. Lakhapatri, S.L.; Abraham, M.A. Analysis of catalyst deactivation during steam reforming of jet fuel on ni-(pdrh)/γ-al2o3 catalyst. *Appl. Catal. A Gen.* **2011**, *405*, 149–159. [CrossRef]
18. Wu, C.; Williams, P.T. Pyrolysis–gasification of plastics, mixed plastics and real-world plastic waste with and without ni–mg–al catalyst. *Fuel* **2010**, *89*, 3022–3032. [CrossRef]
19. Wu, C.; Williams, P.T. Hydrogen production by steam gasification of polypropylene with various nickel catalysts. *Appl. Catal. B* **2009**, *87*, 152–161. [CrossRef]
20. Gupta, R.P.; Turk, B.S.; Portzer, J.W.; Cicero, D.C. Desulfurization of syngas in a transport reactor. *Environ. Prog.* **2001**, *20*, 187–195. [CrossRef]
21. Papurello, D.; Chiodo, V.; Maisano, S.; Lanzini, A.; Santarelli, M. Catalytic stability of a ni-catalyst towards biogas reforming in the presence of deactivating trace compounds. *Renew. Energy* **2018**, *127*, 481–494. [CrossRef]
22. Elbaba, I.F.; Wu, C.; Williams, P.T. Hydrogen production from the pyrolysis–gasification of waste tyres with a nickel/cerium catalyst. *Int. J. Hydrog. Energy* **2011**, *36*, 6628–6637. [CrossRef]
23. Sigot, L.; Ducom, G.; Germain, P. Adsorption of hydrogen sulfide (h2s) on zeolite (z): Retention mechanism. *Chem. Eng. J.* **2016**, *287*, 47–53. [CrossRef]
24. Bandosz, T.J. Effect of pore structure and surface chemistry of virgin activated carbons on removal of hydrogen sulfide. *Carbon* **1999**, *37*, 483–491. [CrossRef]
25. Papurello, D.; Tomasi, L.; Silvestri, S.; Santarelli, M. Evaluation of the wheeler-jonas parameters for biogas trace compounds removal with activated carbons. *Fuel Process. Technol.* **2016**, *152*, 93–101. [CrossRef]
26. Gandiglio, M.; Lanzini, A.; Santarelli, M.; Acri, M.; Hakala, T.; Rautanen, M. Results from an industrial size biogas-fed sofc plant (the demosofc project). *Int. J. Hydrog. Energy* **2020**, *45*, 5449–5464. [CrossRef]
27. Papurello, D.; Gandiglio, M.; Lanzini, A. Experimental analysis and model validation on the performance of impregnated activated carbons for the removal of hydrogen sulfide (h2s) from sewage biogas. *Processes* **2019**, *7*, 548. [CrossRef]
28. Papurello, D.; Gandiglio, M.; Kafashan, J.; Lanzini, A. Biogas purification: A comparison of adsorption performance in d4 siloxane removal between commercial activated carbons and waste wood-derived char using isotherm equations. *Processes* **2019**, *7*, 774. [CrossRef]
29. Hussain, M.; Abbas, N.; Fino, D.; Russo, N. Novel mesoporous silica supported zno adsorbents for the desulphurization of biogas at low temperatures. *Chem. Eng. J.* **2012**, *188*, 222–232. [CrossRef]
30. Song, H.S.; Park, M.G.; Ahn, W.; Lim, S.N.; Yi, K.B.; Croiset, E.; Chen, Z.; Nam, S.C. Enhanced adsorption of hydrogen sulfide and regeneration ability on the composites of zinc oxide with reduced graphite oxide. *Chem. Eng. J.* **2014**, *253*, 264–273. [CrossRef]
31. Stita, S.; Galera Martínez, M.; Pham Xuan, H.; Pham Minh, D.; Nzihou, A.; Sharrock, P. Metal-doped apatitic calcium phosphates: Preparation, characterization, and reactivity in the removal of hydrogen sulfide from gas phase. *Compos. Interfaces* **2015**, *22*, 503–515. [CrossRef]
32. Balsamo, M.; Cimino, S.; De Falco, G.; Erto, A.; Lisi, L. Zno-cuo supported on activated carbon for h2s removal at room temperature. *Chem. Eng. J.* **2016**, *304*, 399–407. [CrossRef]
33. Hervy, M.; Minh, D.P.; Gerente, C.; Weiss-Hortala, E.; Nzihou, A.; Villot, A.; Le Coq, L. H2s removal from syngas using wastes pyrolysis chars. *Chem. Eng. J.* **2018**, *334*, 2179–2189. [CrossRef]
34. Hernández, S.P.; Chiappero, M.; Russo, N.; Fino, D. A novel zno-based adsorbent for biogas purification in h2 production systems. *Chem. Eng. J.* **2011**, *176*, 272–279. [CrossRef]
35. Huang, C.-C.; Chen, C.-H.; Chu, S.-M. Effect of moisture on h2s adsorption by copper impregnated activated carbon. *J. Hazard. Mater.* **2006**, *136*, 866–873. [CrossRef]
36. Florent, M.; Policicchio, A.; Niewiadomski, S.; Bandosz, T.J. Exploring the options for the improvement of h2s adsorption on sludge derived adsorbents: Building the composite with porous carbons. *J. Clean. Prod* **2020**, *249*, 119412. [CrossRef]
37. Juárez, M.F.-D.; Mostbauer, P.; Knapp, A.; Müller, W.; Tertsch, S.; Bockreis, A.; Insam, H. Biogas purification with biomass ash. *Waste Manag.* **2018**, *71*, 224–232. [CrossRef]
38. Bandosz, T.J. *Activated Carbon Surfaces in Environmental Remediation*; Elsevier: Amsterdam, The Netherlands, 2006.
39. de Arespacochaga, N.; Valderrama, C.; Peregrina, C.; Mesa, C.; Bouchy, L.; Cortina, J. Evaluation of a pilot-scale sewage biogas powered 2.8 kwe solid oxide fuel cell: Assessment of heat-to-power ratio and influence of oxygen content. *J. Power Sources* **2015**, *300*, 325–335. [CrossRef]

40. Rasi, S.; Veijanen, A.; Rintala, J. Trace compounds of biogas from different biogas production plants. *Energy* **2007**, *32*, 1375–1380. [CrossRef]
41. Papurello, D.; Boschetti, A.; Silvestri, S.; Khomenko, I.; Biasioli, F. Real-time monitoring of removal of trace compounds with ptr-ms: Biochar experimental investigation. *Renew. Energy* **2018**, *125*, 344–355. [CrossRef]
42. De Arespacochaga, N.; Valderrama, C.; Mesa, C.; Bouchy, L.; Cortina, J. Biogas deep clean-up based on adsorption technologies for solid oxide fuel cell applications. *Chem. Eng. J.* **2014**, *255*, 593–603. [CrossRef]
43. Papurello, D.; Santarelli, M.; Fiorilli, S. Physical activation of waste-derived materials for biogas cleaning. *Energies* **2018**, *11*, 2338. [CrossRef]
44. Barelli, L.; Bidini, G.; Hernàndez-Balada, E.; Mata-Álvarez, J.; Sisani, E. Performance characterization of a novel fe-based sorbent for anaerobic gas desulfurization finalized to high temperature fuel cell applications. *Int. J. Hydrog. Energy* **2017**, *42*, 1859–1874. [CrossRef]
45. Brunauer, S.; Emmett, P.H.; Teller, E. Adsorption of gases in multimolecular layers. *J. Am. Chem. Soc* **1938**, *60*, 309–319. [CrossRef]
46. Bartholomew, C.H.; Farrauto, R.J. Hydrogen production and synthesis gas reactions. In *Fundamentals of Industrial Catalytic Processes*, 2nd ed.; John Wiley & Sons: Holboken, NJ, USA, 2006; pp. 339–486.
47. Gregg, S.; Sing, K. Adsorption, surface area and porosity. Academic press, london. In *Adsorption, Surface Area and Porosity*, 2nd ed.; Academic Press: London, UK, 1982.
48. Fenouil, L.A.; Lynn, S. Study of calcium-based sorbents for high-temperature h2s removal. 2. Kinetics of h2s sorption by calcined limestone. *Ind. Eng. Chem. Res.* **1995**, *34*, 2334–2342. [CrossRef]
49. Nindhia, T.G.T.; Sucipta, I.M.; Surata, I.W.; Adiatmika, I.K.; Negara, D.N.K.P.; Negara, K.M.T. Processing of steel chips waste for regenerative type of biogas desulfurizer. *Int. J. Renew. Energy Res (IJRER)* **2013**, *3*, 84–87.
50. Ducom, G.; Radu-Tirnoveanu, D.; Pascual, C.; Benadda, B.; Germain, P. Biogas–municipal solid waste incinerator bottom ash interactions: Sulphur compounds removal. *J. Hazard. Mater.* **2009**, *166*, 1102–1108. [CrossRef]
51. Sarperi, L.; Surbrenat, A.; Kerihuel, A.; Chazarenc, F. The use of an industrial by-product as a sorbent to remove co2 and h2s from biogas. *J. Environ. Chem. Eng.* **2014**, *2*, 1207–1213. [CrossRef]
52. Wallace, R.; Seredych, M.; Zhang, P.; Bandosz, T.J. Municipal waste conversion to hydrogen sulfide adsorbents: Investigation of the synergistic effects of sewage sludge/fish waste mixture. *Chem. Eng. J.* **2014**, *237*, 88–94. [CrossRef]
53. Asaoka, S.; Okamura, H.; Morisawa, R.; Murakami, H.; Fukushi, K.; Okajima, T.; Katayama, M.; Inada, Y.; Yogi, C.; Ohta, T. Removal of hydrogen sulfide using carbonated steel slag. *Chem. Eng. J.* **2013**, *228*, 843–849. [CrossRef]
54. Sing, K.S. Reporting physisorption data for gas/solid systems with special reference to the determination of surface area and porosity (recommendations 1984). *Pure Appl. Chem.* **1985**, *57*, 603–619. [CrossRef]
55. ALOthman, Z. A review: Fundamental aspects of silicate mesoporous materials. *Materials* **2012**, *5*, 2874–2902. [CrossRef]
56. Zhang, Y.S.; Lu, X.; Owen, R.E.; Manos, G.; Xu, R.; Wang, F.R.; Maskell, W.C.; Shearing, P.R.; Brett, D.J. Fine structural changes of fluid catalytic catalysts and characterization of coke formed resulting from heavy oil devolatilization. *Appl. Catal. B* **2020**, *263*, 118329. [CrossRef]
57. Wang, R.; Sang, S.; Zhu, D.; Liu, S.; Yu, K. Pore characteristics and controlling factors of the lower cambrian hetang formation shale in northeast jiangxi, china. *Energ Explor. Exploit.* **2018**, *36*, 43–65. [CrossRef]
58. Shao, L.; Liu, L.; Wen, H.; Li, Y.; Zhang, W.; Li, M. Characteristics and influencing factors of nanopores in the middle jurassic shimengou shale in well yq-1 of the northern qaidam basin. *Earth Sci. Front.* **2016**, *23*, 164–173.
59. Broekhoff, J. Mesopore determination from nitrogen sorption isotherms: Fundamentals, scope, limitations. In *Studies in Surface Science and Catalysis*; Elsevier: Amsterdam, The Netherlands, 1979; Volume 3, pp. 663–684.
60. Lowell, S.; Shields, J.E.; Thomas, M.A.; Thommes, M. *Characterization of Porous Solids and Powders: Surface Area, Pore Size and Density*; Springer Science & Business Media: Dordrechat, The Netherlands, 2012; Volume 16.